Available online at www.sciencedirect.com
ScienceDirect
Trans. Nonferrous Met. Soc. China 30(2020) 2394−2412
Transactions of Nonferrous Metals Society of China
www.tnmsc.cn

Microstructure and mechanical properties of TiC nanoparticle-reinforced Mg−Zn−Ca matrix nanocomposites processed by combining multidirectional forging and extrusion

Kai-bo NIE[1], Zhi-hao ZHU[1], Paul MUNROE[2], Kun-kun DENG[1], Ya-chao GUO[1]

1. College of Materials Science and Engineering, Taiyuan University of Technology, Taiyuan 030024, China;
2. School of Materials Science and Engineering, University of New South Wales, Sydney, NSW 2052, Australia

Received 9 January 2020; accepted 19 June 2020

Abstract: TiC nanoparticle-reinforced Mg−4Zn−0.5Ca matrix nanocomposites were processed by combining multidirectional forging (MDF) and extrusion (EX). The grain size of the nanocomposite after MDF+EX multi-step deformation was significantly decreased compared with that processed only by MDF. The average size of the recrystallized grains gradually increased after EX with increasing the number of MDF passes at 270 °C. However, the grain size significantly decreased by MDF processing at 310 °C. Both fine and coarse $MgZn_2$ phases appeared in the (MDF+EX)-processed nanocomposites, and their volume fractions gradually increased with increasing the number of MDF passes before EX. Ultrahigh tensile properties (yield strength of ~404 MPa, ultimate tensile strength of ~450.3 MPa and elongation of ~5.2 %) were obtained in the nanocomposite after three MDF passes at 310 °C followed by EX. This was attributed to the refinement of the recrystallized grains, together with the improved Orowan strengthening provided by the precipitated $MgZn_2$ particles that were generated by MDF+EX multi-step deformation.
Key words: magnesium matrix nanocomposite; multi-step deformation; multidirectional forging; mechanical properties; $MgZn_2$ phases

1 Introduction

Particulate-reinforced magnesium matrix composites (PMMCs) have attracted much attention due to their attractive properties, such as high elastic modulus, high strength and high wear resistance [1−3]. Among the various particulate reinforcements that can be used, the addition of nanoscale particles to a magnesium matrix can lead to a higher strengthening increment relative to micron or submicron scale particles, since the number of nano-sized particles is greater than that for micron- or submicron-sized particles at the same volume fraction [4−6]. Furthermore, the generation of dislocations and, hence, strain hardening can be promoted by the addition of nanoparticles. Finally, finer, nanoscale particles are less likely to act as crack initiation sites than coarser particles [7,8]. Thus, there is usually a simultaneous improvement in both strength and ductility of magnesium matrices through nanoparticle additions.

The key to realizing these advantages for magnesium matrix nanocomposites is to generate a homogenous distribution of nanoparticles in the matrix. However, the agglomeration of nano-sized

Foundation item: Projects (51771129, 51401144, 51771128) supported by the National Natural Science Foundation of China, Project supported by the Outstanding Innovative Teams of Higher Learning Institutions of Shanxi, China; Projects (2015021067, 201601D011034) supported by the Natural Science Foundation of Shanxi Province, China; Project (201703D421039) supported by the International Cooperation in Shanxi, China; Project supported by the China Scholarship Council
Corresponding author: Kai-bo NIE, Tel: +86-18334737932, Fax: +86-351-6018051, E-mail: niekaibo@tyut.edu.cn, kaibo.nie@gmail.com; Paul MUNROE, E-mail: p.munroe@unsw.edu.au
DOI: 10.1016/S1003-6326(20)65387-0

particles and the formation of micro-voids in an as-cast magnesium matrix usually act to decrease mechanical properties, and so inhibit practical application [9−11]. As such, the secondary deformation methods including extrusion, forging and rolling have been employed to further improve the mechanical properties of the as-cast nano-composites [4,12−16]. KHOSROSHAHI et al [15] demonstrated that the distribution of SiC nanoparticles was uniform in a SiC_p/AZ80 nanocomposite after hot extrusion and, subsequently, its mechanical properties were enhanced. NIE et al [16] also showed that the agglomeration of SiC nanoparticles could be decreased in the as-extruded nanocomposites by increasing the extrusion temperature, with a concomitant increase in tensile strength. Furthermore, forging has also been shown to eliminate porosity and improve particle distribution, leading to an increase in strength [14,17,18]. Recently, a combination of different deformation methods (multi-step deformation) has been used to process magnesium alloys, such that mechanical properties after multi-step deformation were higher than those after single-step processing [19−21]. QIAO et al [22] processed a nano-SiC_p/AZ91 composite by combining extrusion (EX) and equal channel angular processing (ECAP). The yield strength of this composite was further increased from 245 MPa, in the as-extruded condition, to 328 MPa after EX+ECAP multi-step deformation. WU et al [23] found that the grain size of a cast SiC_p/AZ91 composite was reduced from 37.1 to 9 μm after employing a forging process, which was further decreased to 2.7 μm after subsequent extrusion. Above all, as a potential deformation process for commercial alloys, the application of multi-step deformation can significantly improve the mechanical properties of magnesium matrix nanocomposites.

In our previous work, the combination of semi-solid stirring and ultrasonic vibration was successfully applied to fabricating a TiC_p/Mg−4Zn−0.5Ca nanocomposite [5,24]. After single extrusion, excellent mechanical properties (yield strength (YS) of ~355.3 MPa and ultimate tensile strength (UTS) of ~385.7 MPa) were obtained in a nanocomposite extruded at an extrusion speed of 0.01 mm/s at a low extrusion temperature of 190 °C [5]. These properties were significantly improved relative to the as-cast composites. Furthermore, among the possible deformation approaches, multi-directional forging (MDF) is considered to be highly suitable for use as a pre-deformation step in multi-step deformation relative to other more conventional processing technologies. This is because there is no significant change in the shape of the samples before and after MDF [14]. Previous research [25] has shown that the stored deformation energy of a Mg−4Zn−0.5Ca alloy after 1 MDF pass can promote the nucleation and growth of recrystallized grains during subsequent extrusion. This can lead to clear improvements in the mechanical properties of this alloy. However, to the authors' knowledge, there has been no study focused on the influence of MDF process variables (i.e. deformation temperature or number of MDF passes) on the microstructure and tensile properties of Mg−4Zn−0.5Ca matrix nanocomposites following subsequent extrusion.

In this study, a TiC nanoparticle reinforced Mg−4Zn−0.5Ca nanocomposite was processed by isothermal MDF at two different temperatures (270 °C and 310 °C), followed by EX at 190 °C at an extrusion speed of 0.01 mm/s. The effect of MDF+EX multi-step deformation on the microstructures and mechanical properties of the nanocomposites was systematically investigated.

2 Experimental

2.1 Materials

The matrix alloy used was a Mg−Zn−Ca alloy containing 4% Zn and 0.5% Ca (mass fraction). TiC particles, with mean diameter of 50 nm and a mass fraction of 0.5%, were used as reinforcement. The prepared nanocomposite was denoted as TiC_p/Mg−4Zn−0.5Ca. The morphology of the TiC nanoparticles is presented in Fig. 1.

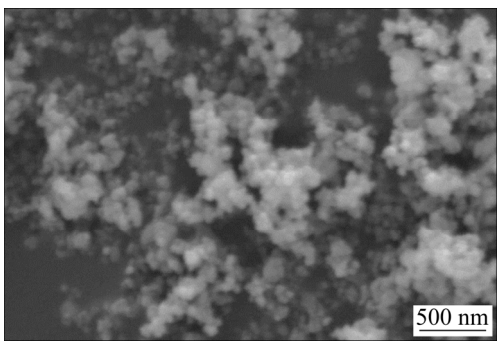

Fig. 1 Morphology of TiC nanoparticles

2.2 Multi-step deformation

Figure 2 shows the process route for the preparation of the TiC_p/Mg−4Zn−0.5Ca nanocomposite. Firstly, nanocomposite billets were fabricated by combining semisolid stirring and ultrasonic vibration as shown in Fig. 2(a). The fabrication process has been described in Ref. [5]. Subsequently, MDF samples were cut from the nanocomposite billets with dimensions of 30 mm × 30 mm × 60 mm. The MDF samples were then homogenized at 320 °C for 8 h, followed by solution treatment at 430 °C for 16 h, and then quenched into water. Before forging, each billet, following removal of any external oxide layer, was pre-heated to a temperature in a range of 270−310 °C for 0.5 h based on the different MDF temperatures employed. The MDF process was performed at two temperatures (270 and 310 °C) with a pressing speed of 2.4 mm/s, using a press with a 315 kN load limit. A schematic diagram of the MDF process is given in Fig. 2(b). The samples were maintained at a dimensional ratio of 1:1:2 during MDF, although the loading direction was rotated by 90° from pass to pass. The TiC_p/Mg−4Zn−0.5Ca nanocomposites processed by isothermal MDF at either 270 °C or 310 °C were named as MDF270 and MDF310, respectively. Samples subjected to multiple passes were named as 3MDF270, for example, to indicate that the composite had been subjected to three passes. Finally, the forged nanocomposites were extruded at 190 °C at a ram speed of 0.01 mm/s with an extrusion ratio of 16:1. The nanocomposite samples after the MDF+EX multi-step deformation process were named as MDF270+EX and MDF310+EX, respectively. A set temperature was maintained for 20 min for each sample before deformation.

2.3 Microstructural characterization

The microstructures of the nanocomposites before and after MDF+EX multi-step deformation were characterized by optical microscopy (OM), scanning electron microscopy (SEM) with energy dispersive spectroscopy (EDS). The phase compositions were determined using X-ray diffraction (XRD) and transmission electron microscopy (TEM, JEM−2100(HR)). XRD analysis was performed using Cu K_α radiation with a scanning speed of 2(°)/min over a range of 2θ angles from 20° to 80° and the pattern was analyzed by MDI Jade 6.0 software. TEM specimens were prepared by mechanical polishing (to ~40 μm) and ion-milling to perforation using a GATAN691 miller at an ion accelerating voltage of 3 kV.

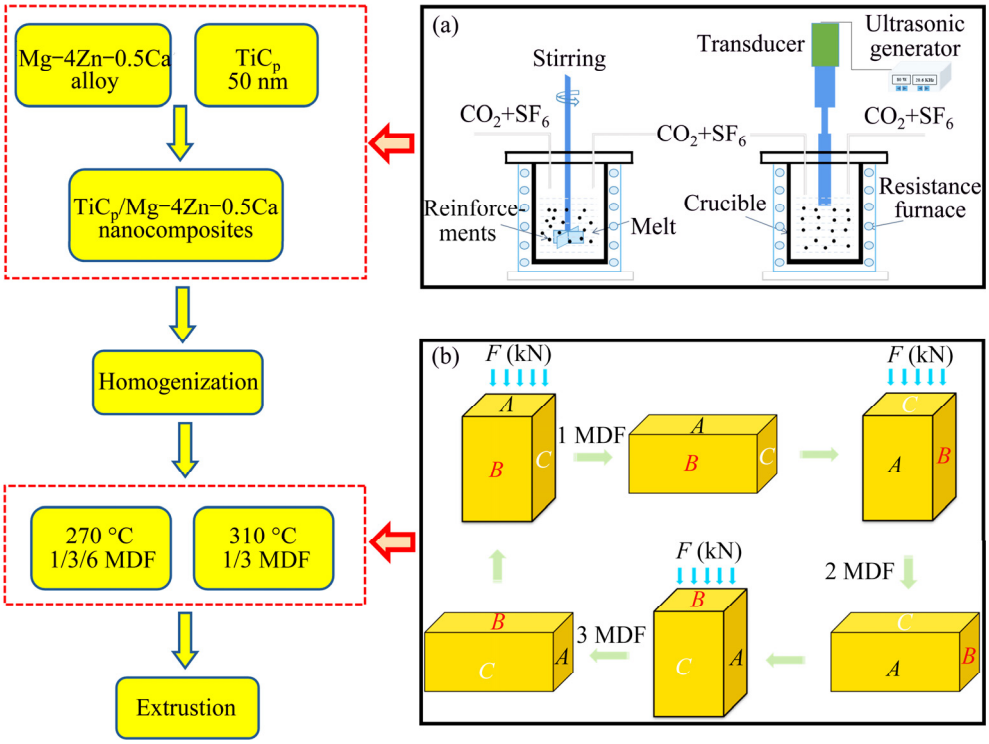

Fig. 2 Process flow for TiC_p/Mg−4Zn−0.5Ca nanocomposites: (a) Combination of semisolid stirring and ultrasonic vibration; (b) Schematic of multidirectional forging

Samples for OM, SEM and XRD analyses were cut in the central region parallel to the forging axis after MDF and along the extrusion direction after MDF+EX multi-step deformation. The specimens for OM were ground and etched by an oxalic acid solution (4 g oxalic + 100 mL H_2O). The average sizes and volume fractions of the dynamic recrystallized (DRXed) grains and the precipitates after multi-step deformation were determined using Image-Pro Plus (IPP) software.

2.4 Tensile properties

Tensile tests were performed on an Instron Series 3369 test machine, where the size of the tensile specimens was 15 mm in gauge length with 6 mm × 2 mm in cross-sectional areas. The tensile speed was set as 0.5 mm/min and the strain rate was 5.6×10^{-4} s^{-1}. To increase the validity of the data, at least three tensile specimens, parallel to extrusion direction, were tested for each process condition.

3 Results

3.1 Microstructures of TiC_p/Mg−4Zn−0.5Ca nanocomposites after MDF270 and MDF270+EX processing

Figure 3(a) shows the XRD analysis of the TiC_p/Mg−4Zn−0.5Ca nanocomposites after the homogenization treatment, 1MDF270 and 1MDF270+EX processing. Higher resolution images of regions *A* and *B* in Fig. 3(a) are given in Figs. 3(b) and (c), respectively. Compared with the as-homogenized TiC_p/Mg−4Zn−0.5Ca nanocomposite, peaks for the $MgZn_2$ phase can be observed after both MDF and MDF+EX multi-step deformation as shown in Fig. 3(b), indicating the occurrence of dynamic precipitation of the $MgZn_2$ phase during MDF and MDF+EX multi-step deformation. Furthermore, peaks for TiC can be clearly found for all the samples as shown in Fig. 3(c).

Figure 4 shows TEM micrograph of the TiC_p/Mg−4Zn−0.5Ca nanocomposite after homogenization treatment. It can be seen that some nanoparticles (indicated by red-crosses) are reasonably uniformly distributed within the matrix (Fig. 4(a)). These particles were confirmed as TiC_p by selected area electron diffraction (Fig. 4(b)). Figure 5 shows a secondary electron image of the TiC_p/Mg−4Zn−0.5Ca nanocomposite after 1 MDF pass at 270 °C. A coarse phase appears in

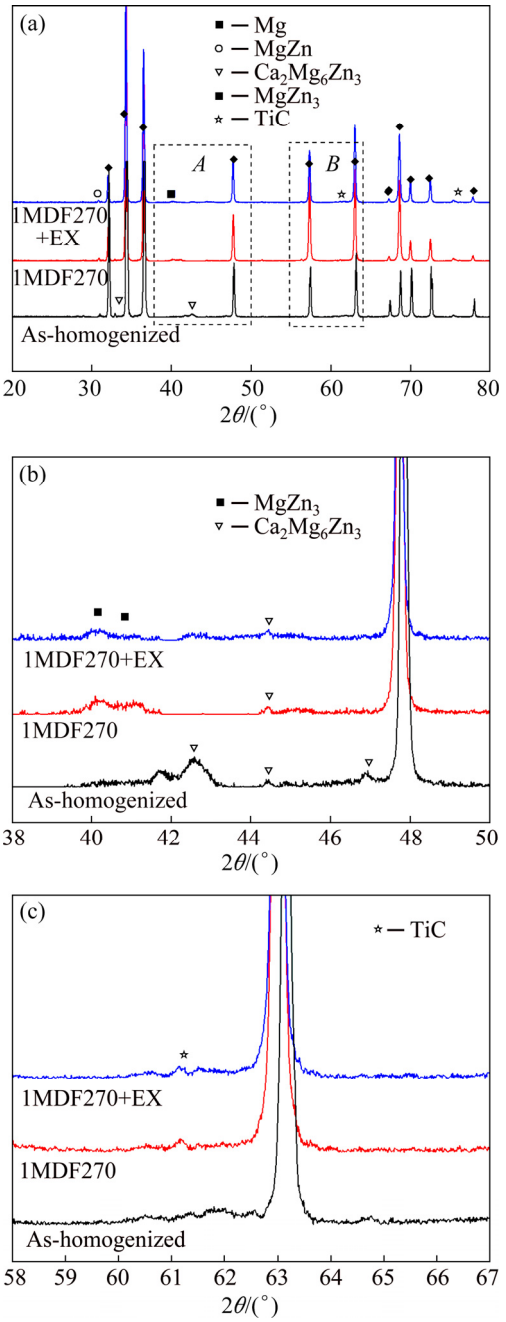

Fig. 3 XRD patterns of TiC_p/Mg−4Zn−0.5Ca nanocomposites under different conditions (a) and high resolution scans (b, c) for regions *A* and *B* in (a), respectively

1MDF270 (marked by yellow arrows, *A*), which exhibits a Zn concentration of 66.6 at.% through EDS analysis (Fig. 5(b)) and is likely a MgZn phase, when considered in combination with the XRD results. Additionally, the fine fractured particles distributed along the extrusion direction mainly contain Mg, Zn and Ca, which suggests that they are $Ca_2Mg_6Zn_3$ phases.

Figure 6 shows optical microstructures of the nanocomposites for specimens following different MDF passes at 270 °C (MDF270). The grain sizes and volume fractions of recrystallized grains in the nanocomposites gradually increased with increasing the number of MDF passes as shown in Fig. 6. It is clear that after 6 MDF passes the grain size distribution is still uneven in the nanocomposite.

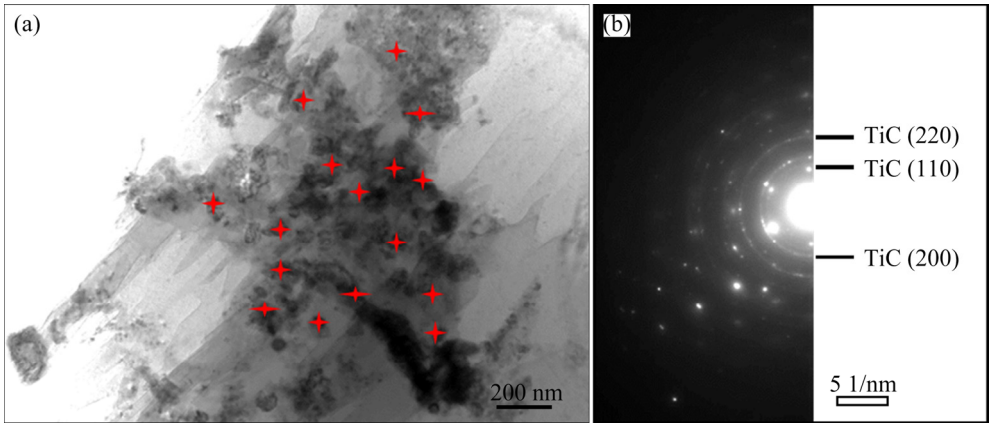

Fig. 4 Bright field TEM image (a) and diffraction pattern showing rings from TiC nanoparticles (b) for as-homogenized TiC_p/Mg−4Zn−0.5Ca nanocomposite

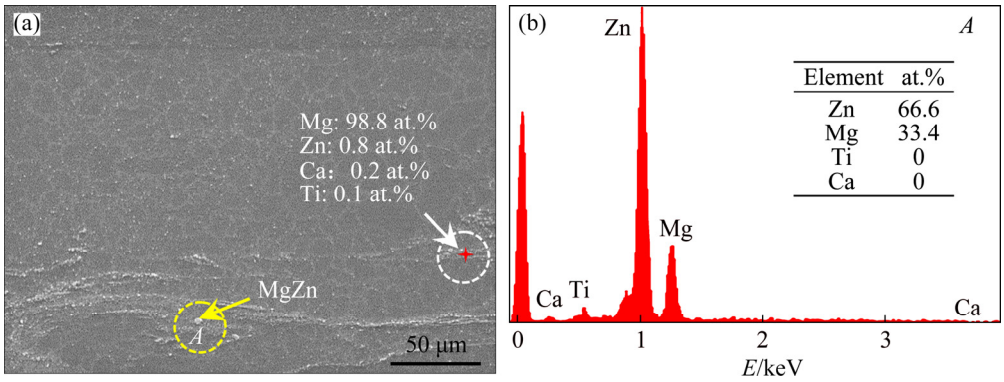

Fig. 5 Secondary electron image of TiC_p/Mg−4Zn−0.5Ca nanocomposite after 1 MDF pass at 270 °C (a) and corresponding EDS analysis (b) from point *A* in (a)

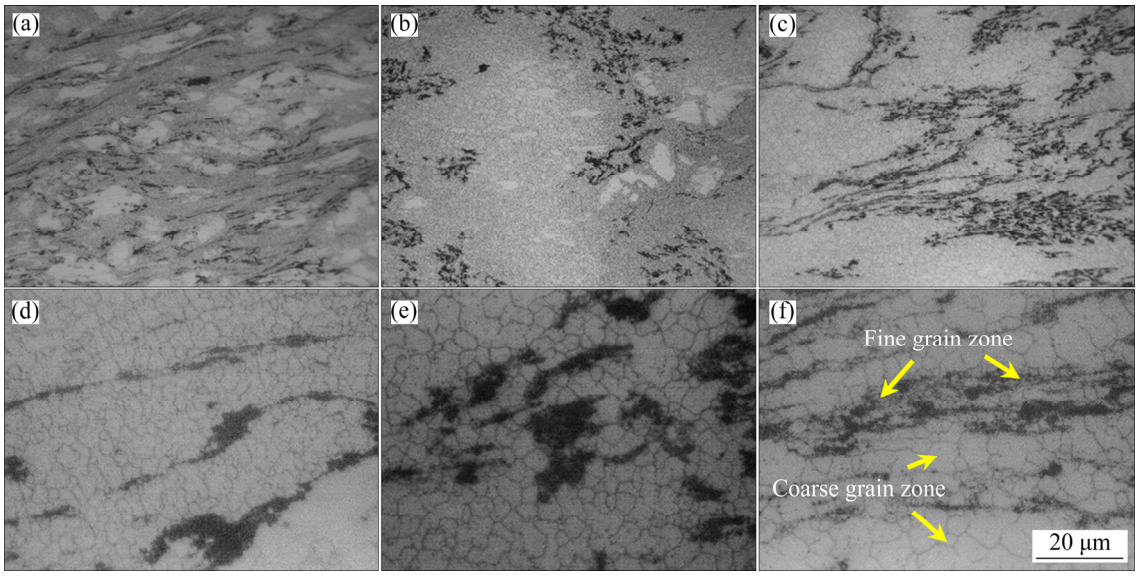

Fig. 6 OM images of TiC_p/Mg−4Zn−0.5Ca nanocomposites after different MDF passes at 270 °C: (a, d) 1 pass; (b, e) 3 passes; (c, f) 6 passes

For example, there is a heterogenous structure consisting of both coarse and fine grains after 6 passes (marked in Fig. 6(f)).

The MDF270 nanocomposites were then subjected to hot extrusion at 190 °C, which are denoted as the MDF270+EX nanocomposites. Figure 7 shows the OM images and size distributions of the DRXed grains in the nanocomposites after MDF270+EX multi-step deformation. The grain size is much smaller relative to the MDF270 nanocomposite. This can be attributed to further dynamic recrystallization occurring during the extrusion process. The average sizes (d_{DRX}) and volume fraction (V_{DRX}) of DRXed grains for the MDF270+EX nanocomposites are listed in Table 1. An increase in the number of MDF passes before extrusion leads to a gradual enhancement of both d_{DRX} and V_{DRX} of the nanocomposites. d_{DRX} increases from 0.64 to 0.76 μm, while the V_{DRX} increases from 86% to 99% as the number of MDF passes increases from 1 to 6.

In order to observe the presence of second phases in the nanocomposites after MDF270+EX multi-step deformation, secondary electron images were used to analyze the fine DRXed grain regions as illustrated in Fig. 8. As can be seen from Figs. 8(a)−(c), there is a large volume fraction of coarse precipitates distributed along the extrusion direction (ED), marked as points *A*, *C* and *E* in the higher magnification images. Moreover, there are a

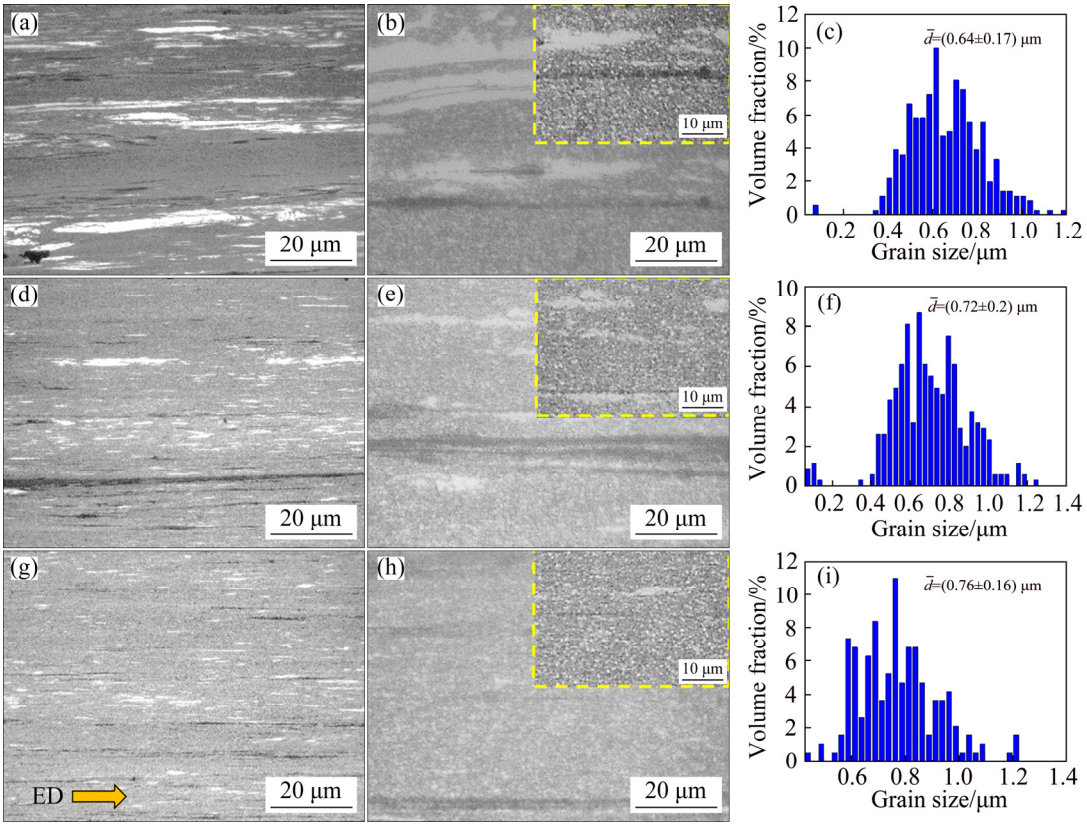

Fig. 7 OM images and DRXed grain size distribution of TiC_p/Mg−4Zn−0.5Ca nanocomposites prepared by MDF270+EX multi-step deformation: (a, b, c) 1MDF270+EX; (d, e, f) 3MDF270+EX; (g, h, i) 6MDF270+EX

Table 1 Microstructural characteristics of TiC_p/Mg−4Zn−0.5Ca nanocomposites fabricated by MDF270+EX multi-step deformation

Deformation mode	DRX		Fine $MgZn_2$		Coarse $MgZn_2$	
	d_{DRX}/μm	V_{DRX}/%	d_p/nm	V_p/%	d_p/nm	V_p/%
1MDF270+EX	0.64	86	54.9	2.5	104.8	2.1
3MDF270+EX	0.72	97	41.9	3.0	130.7	3.1
6MDF270+EX	0.76	99	42.4	3.2	160.1	4.3

V_p: Volume fraction of $MgZn_2$ precipitate

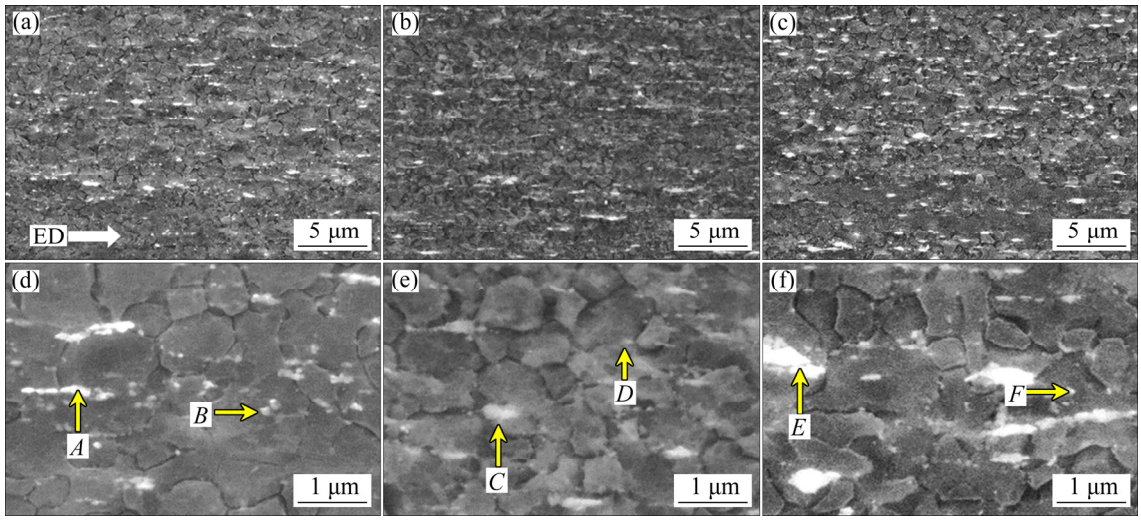

Fig. 8 Secondary electron images of TiC_p/Mg−4Zn−0.5Ca nanocomposites processed by MDF270+EX multi-step deformation: (a, d) 1MDF270+EX; (b, e) 3MDF270+EX; (c, f) 6MDF270+EX

large number of fine secondary phases in the nanocomposites as illustrated at points *B*, *D* and *F*. Both the fine and coarse phases are rich in Mg and Zn based on the results of EDS analysis as given in Table 2. The EDS spectra for points *A*−*F* given in Table 2 are presented in Fig. 9. By combining the EDS data with XRD analysis (Fig. 3), it is clear that $MgZn_2$ precipitates form in the nanocomposites after MDF+EX multi-step deformation. In other words, the compositions of both the fine and coarse precipitates were determined to be $MgZn_2$ phases. The driving force resulting from pre-MDF270 can promote the growth of $MgZn_2$ particles during the extrusion process, resulting in the formation of coarse $MgZn_2$ phases. In addition, under the high strain energy imparted, a large number of fine $MgZn_2$ particles are also precipitated during extrusion. As can be seen from Table 1, the volume fractions (V_p) of these fine $MgZn_2$ precipitates are 2.5%, 3.0% and 3.2% in the 1MDF270+EX, 3MDF270+EX and 6MDF270+EX nanocomposites, respectively, while the V_p for the coarse $MgZn_2$ particles also increases with values of 2.1%, 3.1% and 4.3%, respectively.

Table 2 EDS analysis of TiC_p/Mg−4Zn−0.5Ca nanocomposites fabricated by MDF270+EX multi-step deformation

Point in Fig. 8	Element content/at.%				Possible compound
	Mg	Zn	Ca	Ti	
A	87.3	12.5	0	0.2	$MgZn_2$
B	86.5	13.5	0	0	$MgZn_2$
C	87.8	12.2	0	0	$MgZn_2$
D	90.1	9.3	0.6	0	$MgZn_2$
E	74.8	25.2	0	0	$MgZn_2$
F	82.9	17.1	0	0	$MgZn_2$

3.2 Microstructures of TiC_p/Mg−4Zn−0.5Ca nanocomposites after MDF310 and MDF310+EX

By elevating the MDF temperature to 310 °C before extrusion, the influence of MDF temperature on the microstructure of the TiC_p/Mg−4Zn−0.5Ca nanocomposites was investigated. Figure 10 shows the OM images of the nanocomposites after different MDF passes at 310 °C. The change in the average sizes and volume fractions of DRXed grains is similar to that after single MDF processing at 270 °C. A fully dynamically recrystallized microstructure can be observed in the nanocomposite after 3 MDF passes as shown in Fig. 10(b).

Samples subjected to MDF at 310 °C were then subsequently extruded at 190 °C. Figure 11 gives the OM images and size distributions of the DRXed grains after MDF310+EX multi-step deformation. The corresponding average sizes and volume fractions of the DRXed grains after MDF310+EX multi-step deformation are shown in Table 3. It can be found that the volume fraction and average size of the DRXed grains in the 1MDF310+EX nanocomposite are 79% and

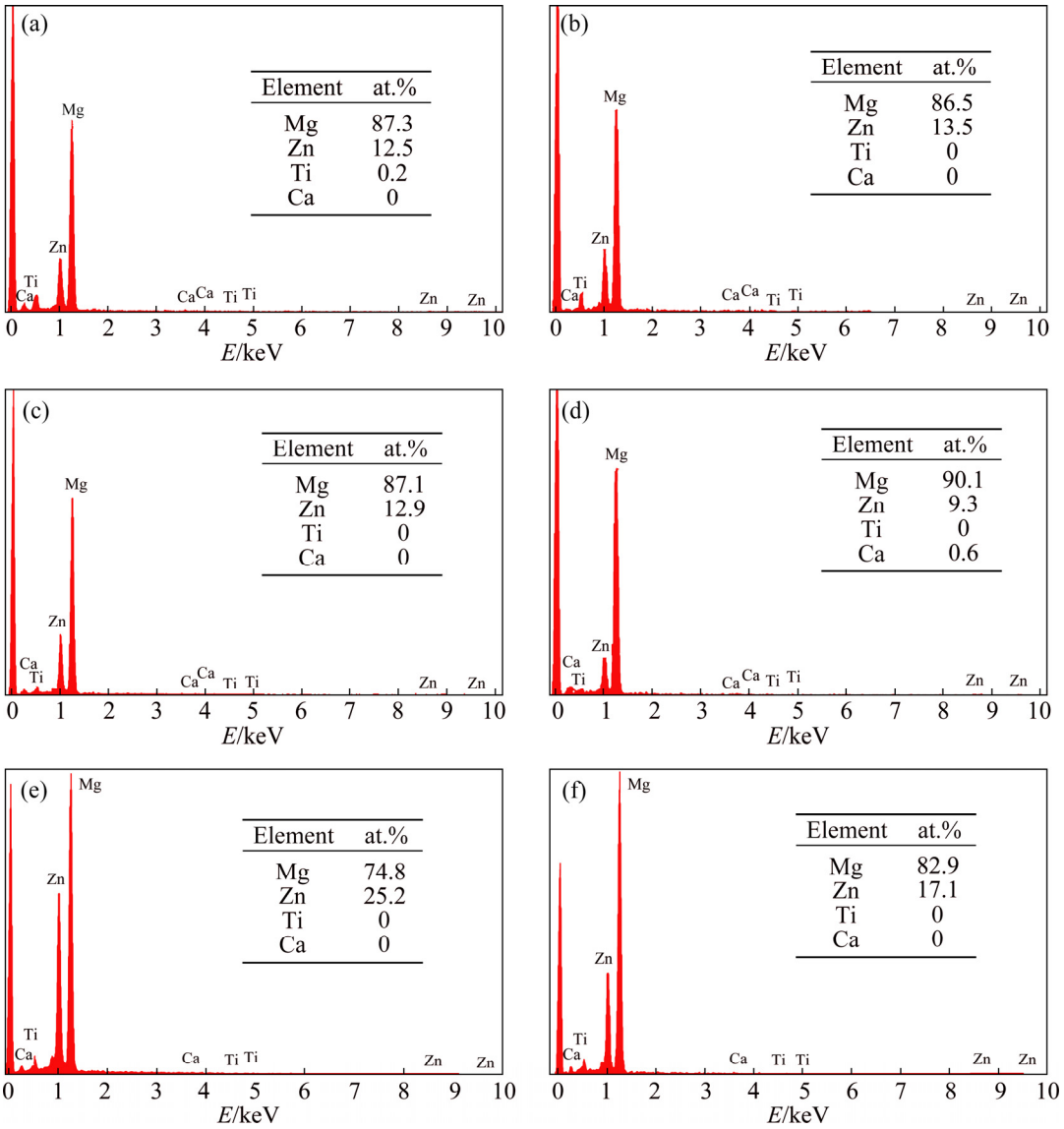

Fig. 9 EDS spectra of points *A*−*F* in Table 2: (a) Point *A*; (b) Point *B*; (c) Point *C*; (d) Point *D*; (e) Point *E*; (f) Point *F*

0.58 μm, respectively. The V_{DRX} of the nanocomposites after 3MDF310+EX multi-step deformation gradually increased to 85%, while the d_{DRX} gradually decreased to 0.40 μm as the number of MDF passes increased before extrusion. Interestingly, there are clear differences in grain size between the MDF310+EX and MDF270+EX nanocomposites.

Figure 12 shows the secondary electron images of the TiC_p/Mg−4Zn−0.5Ca nanocomposites fabricated by MDF310+EX multi-step deformation. It can be found that there are numerous fine and coarse $MgZn_2$ phases in the MDF310+EX nanocomposites and volume fractions of both fine and coarse phases gradually increased with increasing the number of MDF passes before extrusion (as shown in Table 3). These observations are broadly similar to those for the MDF270+EX nanocomposites.

Figure 13(a) shows a TEM micrograph of the TiC_p/Mg−4Zn−0.5Ca nanocomposite after 3MDF310+EX multi-step deformation. It is evident that fine nanoparticles (marked by the yellow circles, e.g., *A*) appear in the 3MDF310+EX sample (Fig. 13(a)), which can be confirmed to be TiC_p by EDS analysis (Fig. 13(b)). In addition, nano-sized precipitates (marked by the white circles, e.g., *B*) can also be observed in the matrix, which can hinder the movement of dislocations. It is evident that the recrystallized grains near the TiC nanoparticles are finer than those far from the TiC nanoparticles as shown in Fig. 13(a).

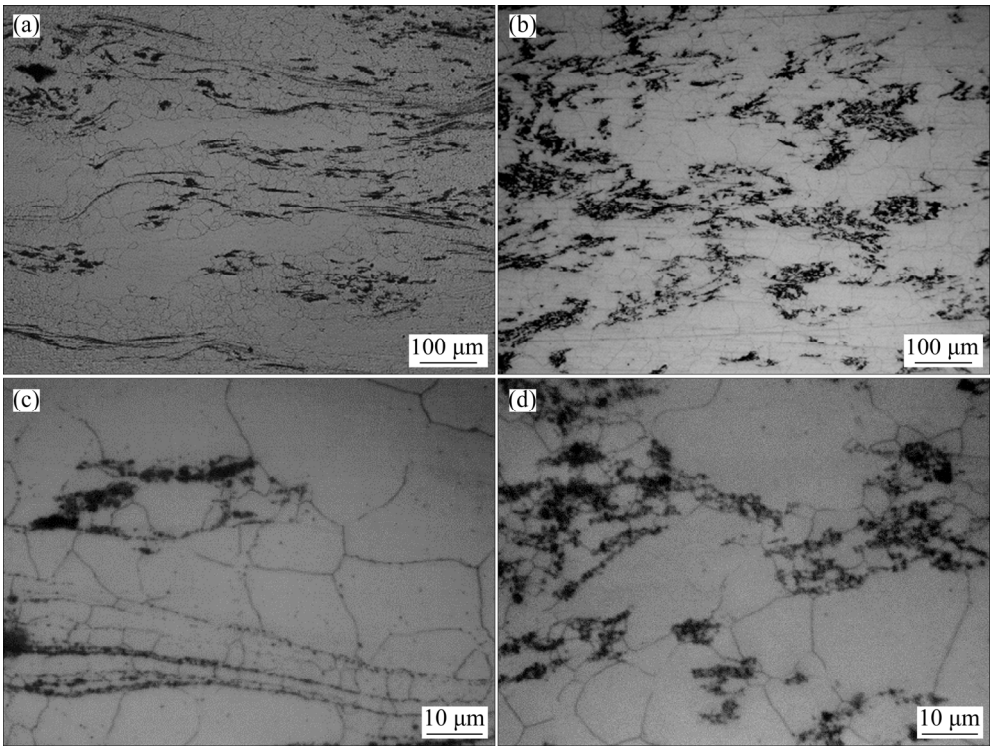

Fig. 10 OM images of TiC_p/Mg−4Zn−0.5Ca nanocomposites for different MDF passes at 310 °C: (a, c) 1 pass; (b, d) 3 passes

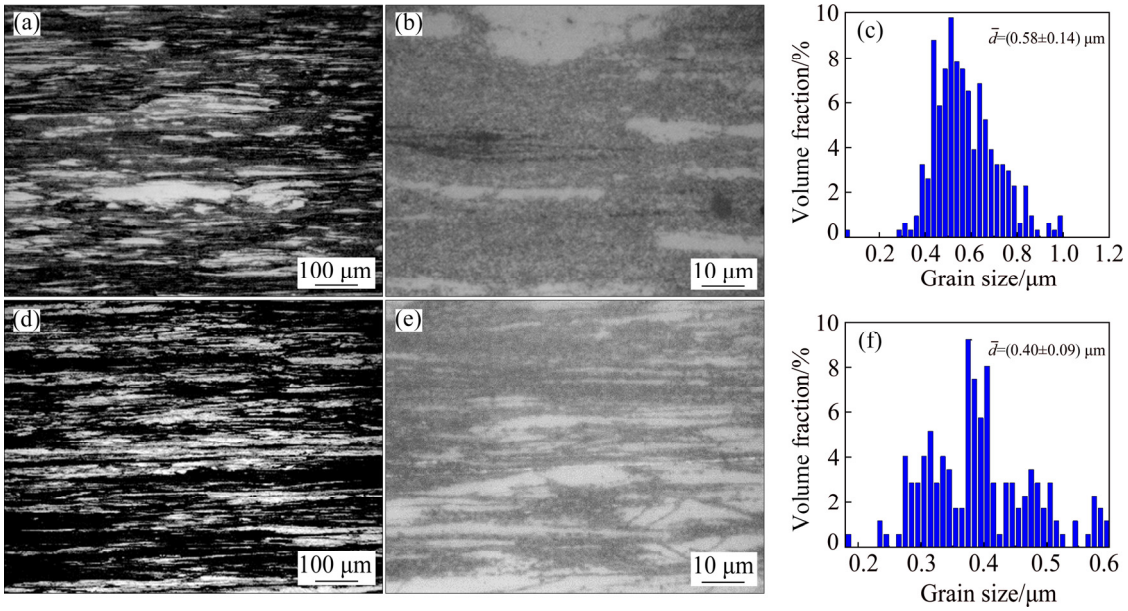

Fig. 11 OM images and grain size distribution of TiC_p/Mg−4Zn−0.5Ca nanocomposites fabricated by MDF310+EX multi-step deformation: (a, b, c) 1MDF310+EX; (d, e, f) 3MDF310+EX

Table 3 Microstructural characteristics of TiC_p/Mg−4Zn−0.5Ca nanocomposites fabricated by MDF310+EX multi-step deformation

Deformation mode	DRX		Fine $MgZn_2$		Coarse $MgZn_2$	
	d_{DRX}/μm	V_{DRX}/%	d_p/nm	V_p/%	d_p/nm	V_p/%
1MDF310+EX	0.58	79	45	3.1	95.7	1.2
3MDF310+EX	0.40	85	40	4.2	136.5	4.1

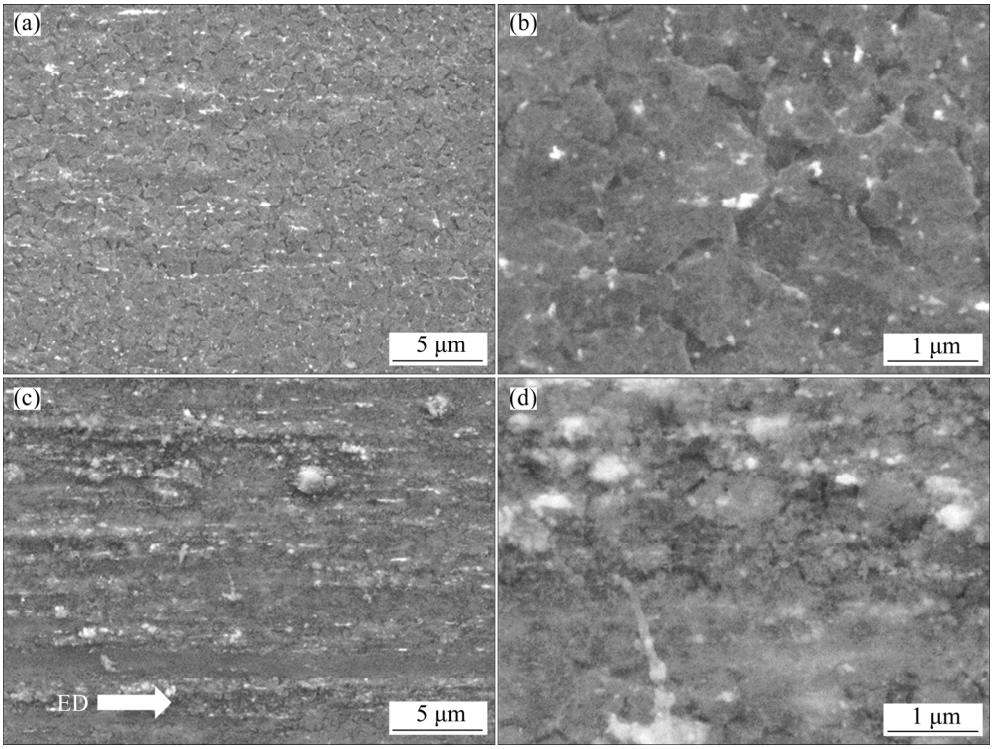

Fig. 12 Secondary electron images of TiC_p/Mg−4Zn−0.5Ca nanocomposites fabricated by MDF310+EX multi-step deformation: (a, b) 1MDF310+EX; (c, d) 3MDF310+EX

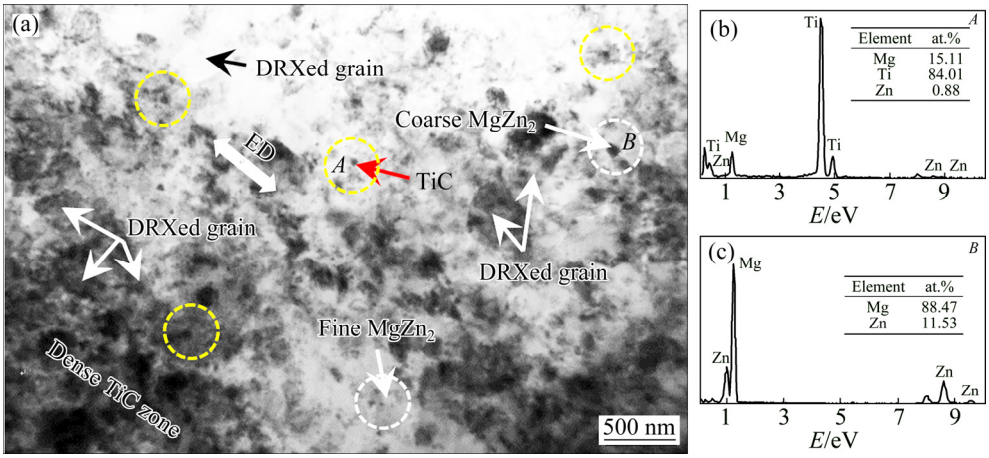

Fig. 13 Transmission electron images of TiC_p/Mg−4Zn−0.5Ca nanocomposite fabricated by 3MDF310+EX: (a) DRXed grains and precipitated phase; (b, c) EDS spectra corresponding to Zones *A* and *B* in (a)

This is because the nano-sized $MgZn_2$ precipitates and externally applied TiC nanoparticles could suppress grain growth due to the Zener pinning effects [26], and thus realizing a fine DRXed grain structure of 0.4 μm.

3.3 Tensile properties of TiC_p/Mg−4Zn−0.5Ca nanocomposites after (MDF+EX) multi-step deformation

Figure 14(a) shows the engineering strain−stress curves of the TiC_p/Mg−4Zn−0.5Ca nanocomposites after MDF270+EX multi-step deformation. Values for yield strength (YS), ultimate tensile strength (UTS) and elongation (EL) are listed in Table 4. It can be seen that YS and UTS in the MDF270+EX nanocomposites exhibit firstly an increase and then a decrease with increasing the MDF passes before extrusion, while the EL shows the opposite trend. A yield strength of ~327.9MPa, ultimate tensile strength of ~372.8 MPa and elongation of ~10.1% were obtained for the 3MDF270+EX nanocomposite. Figure 14(b) shows

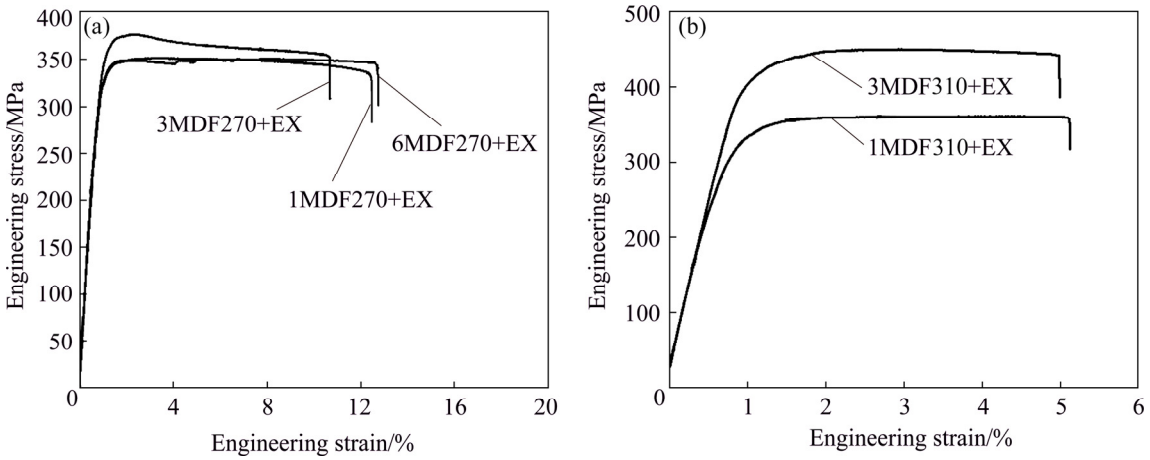

Fig. 14 Engineering strain−stress curves of TiC_p/Mg−4Zn−0.5Ca nanocomposites fabricated by multi-step deformation: (a) MDF270+EX; (b) MDF310+EX

Table 4 Tensile properties of developed TiC_p/Mg−4Zn−0.5Ca nanocomposites after multi-step deformation, and their comparison with previous studies

Material	Deformation	YS/MPa	UTS/MPa	Elongation/%	Source
Nano-TiC_p/Mg−4Zn−0.5Ca	1MDF270+EX	322.7±11.7	343.2±3.5	13.1±4.8	Present work
	3MDF270+EX	327.9±18.1	372.8±4.3	10.1±0.8	Present work
	6MDF270+EX	315.1±7.5	347.8±5.2	13.3±0.8	Present work
	1MDF310+EX	325±9.5	360.5±5.8	5.5±0.8	Present work
	3MDF310+EX	404±12.3	450.3±7.4	5.2±0.6	Present work
	As-cast	~78	~203	~15.4	[24]
	EX (190 °C, 0.01 mm/s)	~355.3	~385.7	~10.2	[5]
Nano-SiC_p/AZ31	EX	~320	~385	~6	[9]
Nano-TiC_p/ZK60	EX	~184	~309	~11.6	[27]
Nano-SiC_p/AZ91	EX	~255	~345	~12	[28]
Nano-SiC_p/AZ31	EX-roll	~250	~310	~9	[4]
Micro-SiC_p/AZ91	Forged-EX	~292	~389	~2.1	[23]
Nano-SiC_p/AZ91	EX-1ECAP	~328	~374	~1.5	[22]

the engineering strain−stress curves of the MDF310+EX nanocomposites. The tensile strength of the 3MDF310+EX nanocomposite is higher relative to the 1MDF310+EX nanocomposite as summarized in Table 4. The 3MDF310+EX nanocomposite exhibited excellent mechanical properties and its YS, UTS and EL were ~404 MPa, ~450.3 MPa and ~5.2%, respectively.

As can be seen from Table 4, the mechanical properties in the nanocomposite after multi-step deformation are higher relative to their as-cast counterpart, which has been described in our previous study [24]. Moreover, compared with the TiC_p/Mg−4Zn−0.5Ca nanocomposites processed by single extrusion in our previous study [5], the YS and UTS values after 3MDF310+EX multi-step deformation were improved by 13.7% and 16.7%, respectively. However, it is worth noting that the YS and UTS of the MDF270+EX and 1MDF310+EX nanocomposites are lower relative to the as-extruded counterpart. This indicates that the MDF temperature has a significant effect on the mechanical properties of the nanocomposites processed by (MDF+EX) multi-step deformation. In addition, the tensile properties of other particles-reinforced magnesium matrix composites are also given for comparison, as shown in Table 4. After 3MDF310+EX multi-step deformation, the optimal

mechanical properties (YS of ~404 MPa and UTS of ~450.3 MPa) of the TiC_p/Mg−4Zn−0.5Ca nanocomposite are improved relative to other magnesium matrix composites deformed by single extrusion or multi-step deformation [4,7,22, 23,27,28,].

4 Discussion

4.1 Microstructures of nanocomposites after MDF+EX multi- step deformation

For the MDF270+EX nanocomposites, both the average sizes and volume fractions of the DRXed grains are increased by increasing the number of MDF passes (as described in Section 3.1). The average sizes and volume fractions of the DRXed grains are affected by both the initial grain size in the different MDF conditions and the extrusion parameters. Since the extrusion parameters were kept constant, variations in the average sizes and volume fractions of the DRXed grains are mainly affected by the initial grain structure. Before extrusion, the larger size and higher volume fraction of DRXed grains obtained in 6MDF270 composite may arise because the recrystallized grains have more time and energy to nucleate and grow with increasing the number of MDF passes [29]. On one hand, compared with 1MDF270 and 3MDF270 composites, deformation of 6MDF270 composite would generate more heat associated with strain energy, which is beneficial to the nucleation and growth of DRXed grains. On the other hand, each billet before each MDF pass was reheated to set temperature for 0.5 h in order to balance the heat, which is also favorable to the growth of DRXed grains. Thus, the average sizes and volume fractions of the DRXed grains in 6MDF270 sample increase with increasing the number of MDF passes. It has been reported that during the subsequent extrusion, the nucleation and growth of DRXed grains can be promoted by the strain energy of materials subjected to MDF as a pre-deformation step [30]. Further, according to the thermodynamics of recrystallization, the reduction of interfacial and strain energy can promote the nucleation of DRXed grains [31−33]. This means that the regions containing large amount of crystal defects, such as dislocations and vacancy clusters, were potential nucleation sites for new grains. Thus, the occurrence of relatively large sizes and high volume fraction of DRXed grains with increasing the number of MDF passes in 6MDF270 sample was thought to promote dynamic recrystallization after extrusion owing to the large number of potential nucleation sites. Accordingly, the grain sizes and volume fractions of 6MDF270+EX composite increase with increasing the number of MDF passes.

With regard to the MDF310+EX nanocomposites, with increasing the number of MDF passes before extrusion, V_{DRX} increased and the d_{DRX} decreased, as described in Section 3.2. Compared with the 1MDF310 nanocomposite, DRX is more complete and there are more grain boundaries in the 3MDF310 nanocomposite, which can then act as locations for nucleation during subsequent extrusion, which in turn promote DRX nucleation and grain refinement [34]. This indicates that the overall surface area of the starting grain boundaries plays a more important role in grain refinement relative to promotion of nucleation through a higher strain energy. However, changes in grain sizes for the MDF310+EX nanocomposite and MDF270+EX nanocomposites are apparently different. Dynamic recrystallization occurs more easily at higher deformation temperatures, which reduces the strain energy of the nanocomposites. Thus, the strain energy in the MDF310 nanocomposites is lower than that in the MDF270 nanocomposites, and its corresponding effect on DRX is reduced for the MDF310 processed materials relative to the MDF270 nanocomposites.

As noted in Sections 3.1 and 3.2, the greater the number of MDF passes before extrusion is, the higher the volume fractions of fine and coarse $MgZn_2$ phases in the MDF+EX nanocomposites are. This can be attributed to the strain energy of nanocomposites after MDF processing, which can promote the formation of fine $MgZn_2$ phases and the coarsening of any pre-existing $MgZn_2$ phases, during the extrusion process.

4.2 Tensile properties

The YS and UTS values of the MDF270+EX nanocomposites firstly increased and then decreased with increasing the number of MDF passes before extrusion, whilst, as expected, variations in EL showed the opposite tendency (as noted in Section 3.3). However, for the

MDF310+EX nanocomposites, the YS and UTS increased with increasing MDF passes, while the EL values decreased slightly. The best mechanical properties (YS ~404 MPa, UTS ~450.3 MPa) were obtained after 3MDF310+EX multi-step deformation. This is presumably due to the strengthening effects of the added TiC nanoparticles, grain refinement as well as the presence of the precipitated phases.

The increased YS contributed by grain refinement can be described by the Hall−Petch relationship [35−37]:

$$\sigma_y=\sigma_0+Kd^{-1/2} \quad (1)$$

where σ_y is the YS, σ_0 is a constant, d is the average grain size, and K is the Hall−Petch slope (≈130 MPa·μm$^{1/2}$) [38]. For the present research, the YS increment for the MDF+EX nanocomposites contributed by grain refinement can be expressed as follows:

$$\Delta\sigma_{\text{Hall–Petch}} = K(d_{\text{as-cast}}^{-1/2} - d_{\text{MDF+ED}}^{-1/2}) \quad (2)$$

where $\Delta\sigma_{\text{Hall–Petch}}$ represents the YS increment owing to grain refinement, $d_{\text{as-cast}}$ is the average grain size in as-cast condition, with a value of about 59.2 μm for the as-cast TiC_p/Mg−4Zn−0.5Ca nanocomposite as shown in our previous study [5]. The parameter $d_{\text{EDF+ED}}$ represents the average grain size after MDF+EX multi-step deformation, and its values are shown in Tables 1 and 3. Therefore, the increments in YS due to grain refinement are 145.6, 136.3 and 132.2 MPa for the 1MDF270+EX, 3MDF270+EX and 6MDF270+EX nanocomposites, respectively. For the MDF310+EX nanocomposites, the $\Delta\sigma_{\text{Hall–Petch}}$ values resulting from grain refinement were calculated as 153.8 and 188.7 MPa for the nanocomposite after 1MDF310+EX and 3MDF310+EX treatment, respectively.

Moreover, the nano-sized particles can impart a strengthening effect via the Orowan mechanism [39,40]. For simplicity, the added TiC nanoparticles and nano-sized $MgZn_2$ precipitates are presumed to be bypassed by dislocations, which gives rise to the Orowan strengthening. The enhancement in YS of the nanocomposites due to the Orowan strengthening ($\Delta\sigma_{\text{Orowan}}$) is given by following equation [41−43]:

$$\Delta\sigma_{\text{Orowan}} = M\frac{0.4Gb}{\pi\sqrt{1-v}}\frac{1}{\left(\sqrt{\frac{\pi}{4f}-1}\right)}\ln\frac{\bar{d}}{b} \quad (3)$$

where M represents the strengthening coefficient given as 1.25 [41], v stands for the Poisson ratio of the matrix alloy (0.35), G represents the shear modulus of the Mg matrix with a value of 16.5 GPa and b stands for the Burgers vector component (0.32 nm) [42]; $\bar{d}$ and f are the average size and volume fraction of the reinforcement particles, respectively. For TiC nanoparticles, the volume fraction was estimated at 0.2%. The volume fraction of the TiC nanoparticles can be calculated by Ref. [44]:

$$\frac{V_{\text{TiC}}}{V_{\text{m}}} = \frac{M_{\text{TiC}}}{M_{\text{m}}}\times\frac{\rho_{\text{m}}}{\rho_{\text{TiC}}} = 0.5\%\times\frac{1.76}{4.93} = 0.18\% \quad (4)$$

where V_{m} and M_{m}, respectively, are the volume fraction and mass fraction of the matrix alloy; ρ_{m} is the density of the matrix alloy (1.76 g/cm^3); M_{TiC} is the mass fraction of TiC (0.5 wt.%) and ρ_{TiC} is the density of TiC (4.93 g/cm^3) [44]. Thus, the volume fraction of applied TiC_p was calculated to be 0.18%, or 0.2% if presented to one decimal point.

According to Eqs. (3) and (4), the increment in YS due to the Orowan strengthening (by TiC_p and $MgZn_2$) for the MDF270+EX and MDF310+EX nanocomposites were calculated and the values are listed in Table 5.

Table 5 Increment in YS due to contributions of TiC_p and $MgZn_2$ precipitates in TiC_p/Mg−4Zn−0.5Ca nanocomposites after MDF+EX multi-step deformation (MPa)

Multi-step deformation	$\Delta\sigma_{\text{TiC}}$	$\Delta\sigma_{\text{coarse}}$	$\Delta\sigma_{\text{fine}}$	$\Delta\sigma_{\text{Orowan}}$
1MDF270+EX	6.6	13.3	25	44.9
3MDF270+EX	6.6	14.1	34.5	55.2
6MDF270+EX	6.6	14.7	35.7	57
1MDF310+EX	6.6	10.4	33.4	50.4
3MDF310+EX	6.6	16.2	46.3	69.1

Note: $\Delta\sigma_{\text{TiC}}$ stands for the Orowan strengthening caused by TiC nanoparticles; $\Delta\sigma_{\text{coarse}}$ and $\Delta\sigma_{\text{fine}}$ are the Orowan strengthening caused by coarse and fine $MgZn_2$ phases, respectively; $\Delta\sigma_{\text{Orowan}}$ is the sum of $\Delta\sigma_{\text{TiC}}$, $\Delta\sigma_{\text{coarse}}$ and $\Delta\sigma_{\text{fine}}$

There also exists a mismatch of the coefficients of thermal expansion (CTE) between TiC_p and the matrix, which can promote the formation of dislocations in the vicinity of the TiC particles that then contribute to an increase in YS. This strengthening mechanism is known as the dislocation strengthening mechanism. The enhancement in YS for these nanocomposites due to

dislocation strengthening ($\Delta\sigma_{CTE}$) can be expressed by following equation [44,45]:

$$\Delta\sigma_{CTE}=\sqrt{3}MGb\sqrt{\frac{12\Delta T\Delta\alpha f_p}{bd_p}} \quad (5)$$

where d_p and f_p are related to the reinforcement particles, especially the average size and volume fraction of TiC nanoparticles in the present work. $\Delta\alpha$ is the difference in CTE values between the TiC nanoparticles and magnesium matrix, the values for TiC and the alloy matrix are 7.4×10^{-6} and 30.7×10^{-6} K^{-1} [44], respectively. ΔT stands for the difference between the tensile test temperature and deformation temperature. According to Eq. (5), the values of $\Delta\sigma_{CTE}$ for the MDF270+EX and MDF310+EX nanocomposites can be both calculated as 27.9 MPa.

Figure 15(a) shows the increment in YS of the MDF270+EX nanocomposites contributed by the strengthening mechanisms arising from grain refinement, Orowan and dislocation strengthening, respectively. The greatest contribution to the increment in YS is attributed to grain refinement with secondary contributions from the Orowan strengthening. In addition, the value of $\Delta\sigma_{Hall-Petch}$ decreases with increasing the number of MDF passes before extrusion, while the $\Delta\sigma_{Orowan}$ increases with the number of passes and $\Delta\sigma_{CTE}$ shows little change. Thus, the YS of MDF270+EX nanocomposites firstly increases and then decreases. For the MDF310+EX nanocomposites, both $\Delta\sigma_{Hall-Petch}$ and $\Delta\sigma_{Orowan}$ increase with an increase in the number of MDF passes before extrusion as shown in Fig. 15(b). As a result, the tensile strength values of the MDF310+EX nanocomposites are gradually increased. The calculated YS is lower than the experimentally determined value. This may be because strengthening effects caused by the contributions of extremely fine precipitated phases observed by TEM (Fig. 12(a)) and back stress strengthening are neglected. The nanocomposites exhibit a mixed structure which consists of both recrystallized regions and deformed regions. To accommodate the incompatibility between fine DRXed grains and coarse deformed grains, geometrically necessary dislocations and back stresses may be generated in the coarse deformed grains, which can generate back stress strengthening [40,46]. ZHANG et al [46] found that a Mg−Al−2Sn−1Zn (wt.%) alloy after extrusion, exhibited a mixed grain microstructure that can generate back stress strengthening during tensile testing. However, due to the lack of a corresponding formula to determine back stress strengthening, no appropriate calculation for YS could be performed for the nanocomposites examined in this study.

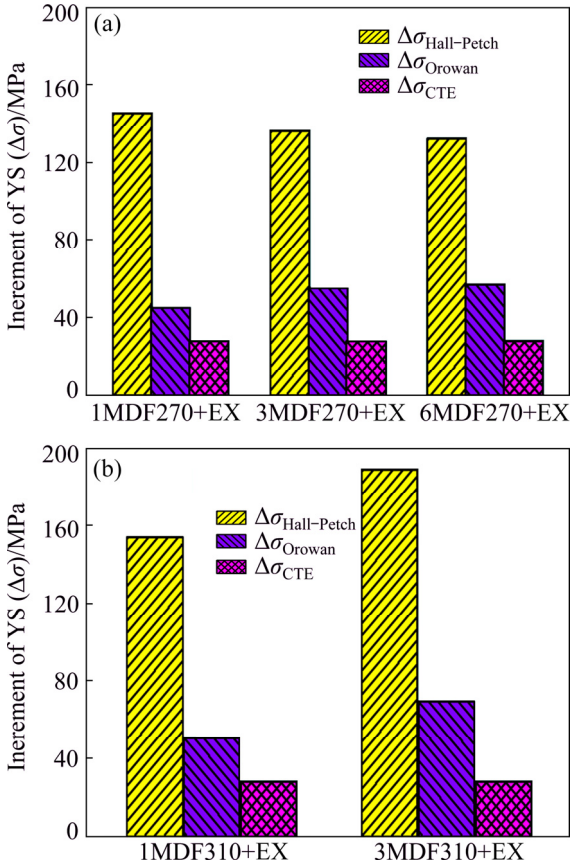

Fig. 15 Theoretical increment of YS due to strengthening mechanisms of grain refinement, Orowan strengthening and dislocation strengthening: (a) MDF270+EX; (b) MDF310+EX

4.3 Influence of deformation processing on microstructure and mechanical properties

As noted in Section 3.3, after 3MDF310+EX multi-step deformation, the nanocomposite exhibited excellent mechanical properties (YS of ~404 MPa, UTS of ~450.3 MPa) relative to other nanocomposites processed by only single extrusion in our previous study [5]. However, the tensile strength of the nanocomposite after 3MDF270+EX multi-step deformation was lower than that of its as-extruded counterpart as shown in Table 4. This can be ascribed to difference in the microstructure of 3MDF270+EX, 3MDF310+EX and the as-extruded nanocomposites, as well as the

difference in the MDF process parameters before extrusion. Both the average grain size (0.72 μm) and DRX volume fraction (97%) of the MDF270+EX nanocomposite are larger relative to the as-extruded nanocomposite (0.34 μm and 73.2%) examined in our previous study [5]. This means that the 3MDF270 nanocomposite treatment before extrusion leads to a high DRX ratio and the growth of DRXed grains in the nanocomposite. The strain energy in the 3MDF270 nanocomposite can promote the nucleation and growth of DRXed grains during subsequent extrusion, resulting in a large grain size and high DRX volume fraction.

For the 3MDF310+EX nanocomposite, the average grain size (0.40 μm) and DRX volume fraction (85%) are lower than those of the 3MDF270+EX nanocomposite. In addition, the volume fraction of DRXed grains in the 3MDF310+EX nanocomposite is higher than that of the as-extruded nanocomposite, but the average DRXed grain size is almost the same. There are more grain boundaries in the 3MDF310 nanocomposites (as noted in Section 4.1), which can serve as nucleation sites for DRX during subsequent extrusion, which thus promotes nucleation and refines the DRXed grains. Moreover, compared with the 3MDF270 nanocomposites, the degree of strain energy in 3MDF310 nanocomposites is lower, which has less effect on DRXed grain growth.

There are a large number of fine and coarse $MgZn_2$ phases in the 3MDF270+EX and 3MDF310+EX nanocomposites, as shown in Tables 1 and 3. During the extrusion process, the strain energy of 3MDF270 and 3MDF310 nanocomposites can promote the formation of fine $MgZn_2$ phases and the growth of the pre-existing $MgZn_2$ particles, resulting in a higher volume fraction of $MgZn_2$ phases relative to the as-extruded nanocomposite (~5.6 vol.%) [5]. Moreover, the volume fraction of $MgZn_2$ particles in the 3MDF310+EX nanocomposite is higher than that of the MDF270+EX nanocomposite. Based on our previous study [5], the YS increment of the nanocomposite processed by single extrusion is derived from a mixture of grain refinement (206.1 MPa), Orowan strengthening (52.3 MPa) and dislocation strengthening (27.9 MPa). A YS value of ~355.3 MPa and UTS of ~385.7 MPa obtained in the as-extruded nanocomposite can be ascribed to both grain refinement (~0.34 μm) and the large volume fraction of precipitated $MgZn_2$ phases (~5.6 vol.%) [5]. In the present work, Orowan strengthening contributed by the $MgZn_2$ precipitates for the 3MDF270+EX nanocomposite is higher than that for the as-extruded nanocomposite, which can be attributed to the higher strain energy in nanocomposite after the 3MDF270 treatment. However, during the subsequent extrusion process, the strain energy can promote the growth of DRXed grains [31], which decreases the contribution to strengthening from grain refinement for the 3MDF270+EX nanocomposite. After 3MDF310+EX multi-step deformation, the grain size of the DRX grains in the nanocomposite is further decreased and the volume fraction of $MgZn_2$ phases is greatly increased, leading to an excellent suite of mechanical properties (YS, UTS and EL were ~404 MPa, ~450.3 MPa and ~5.2%, respectively).

Figure 16 shows tensile fractures of TiC_p/Mg−4Zn−0.5Ca nanocomposites after different MDF+EX multi-step deformation treatments. It can be seen from OM and SEM analysis that twins appear in all the MDF+EX nanocomposites during uniaxial tensile testing at room temperature. $\{10\bar{1}1\}$ contraction twins are readily activated in the latter stages of tensile testing when the *c*-axis is under compression within the coarse unDRXed grains owing to their reduced critical resolved stress [47], which can act as source of cracks leading to premature failure. As shown in Fig. 16(a), there are a large number of twins present in the coarse deformed regions of the 3MDF310+EX nanocomposite. Dislocation pile-up occurs at twin boundaries during uniaxial tensile testing, resulting in the generation of local stress concentrations stimulating the nucleation of microcracks. Then, the microcracks propagate, resulting in final fracture, which reduces the UTS and elongation to failure of the nanocomposite. From the high-magnification SEM image in Fig. 16(c), there are many cracks in the twinned grains and cleavage planes and a few dimples (shown by the red dotted box, in Fig. 16(c)) in the 3MDF310+EX sample, which exhibits decreased ductility. In contrast, the number of twins in 6MDF270+EX sample (Fig. 16(f)) is much less than the other samples (Figs. 16(b−e)), and the

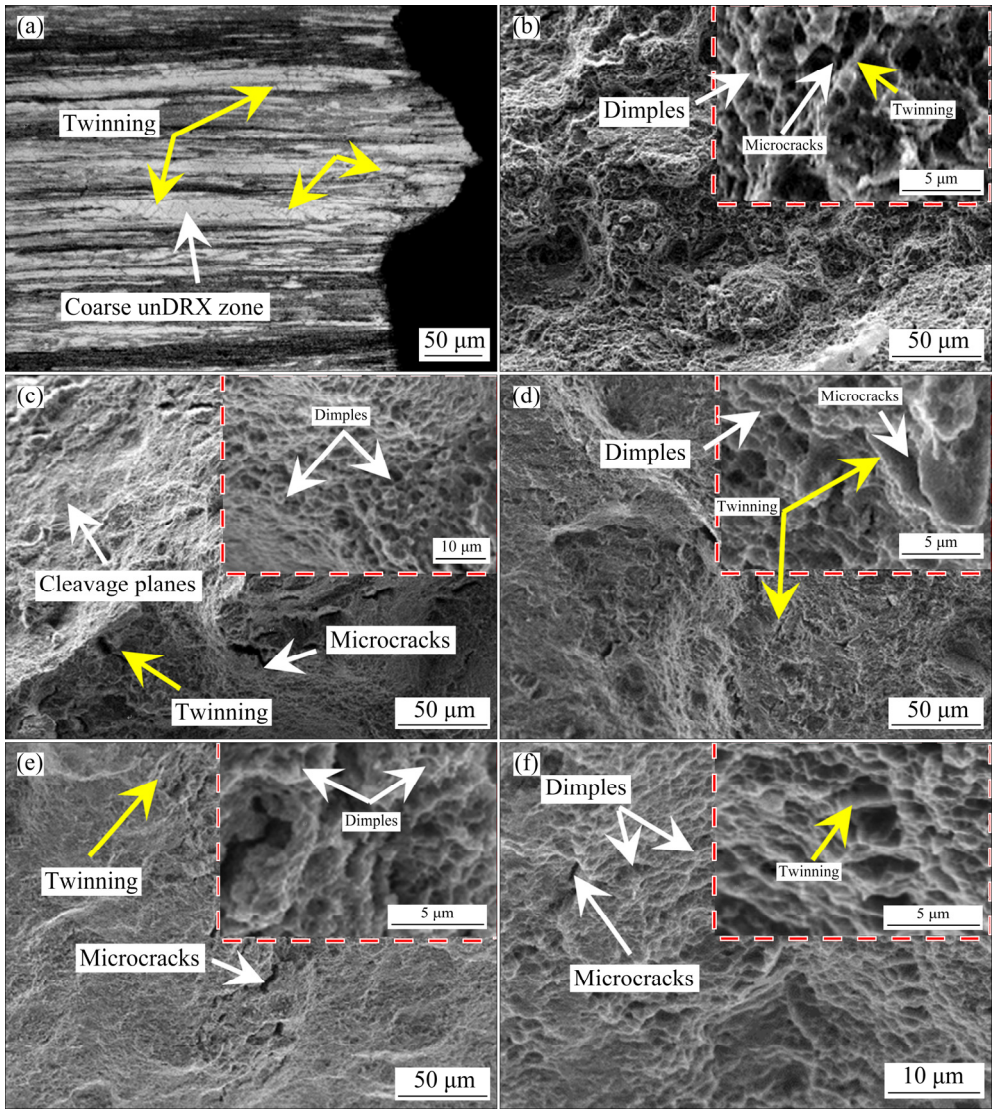

Fig. 16 OM image of near-fracture surfaces (a) and secondary electron images for TiC_p/Mg−4Zn−0.5Ca nanocomposites after different MDF+EX multi-step deformation (b−f): (a, c) 3MDF310+EX; (b) 1MDF310+EX; (d) 1MDF270+EX; (e) 3MDF270+EX; (f) 6MDF270+EX

DRX volume fraction was significantly improved (V_{DRX}=99%, as shown in Table 1). Thus, the 6MDF270+EX sample possesses the maximum EL (13.3%) among all the MDF+EX nanocomposites. Further, from the high-magnification SEM image, dimples, as well as microcracks, were also observed in all samples (Figs. 16(b−f)). Accordingly, the fracture mechanism for the MDF+EX sample is a mixture of dimple fracture and cracking along the twins.

5 Conclusions

(1) The grains in the TiC_p/Mg−4Zn−0.5Ca nanocomposite after MDF+EX multi-step deformation are significantly refined compared with the nanocomposite after MDF processing only. With increasing the number of MDF passes before extrusion, d_{DRX} gradually increased for the MDF270+EX nanocomposites, whilst an opposite trend was observed for the MDF310+EX nanocomposites.

(2) Both volume fractions of the fine and coarse $MgZn_2$ phases are gradually increased with increasing the number of MDF passes before extrusion. This can be attributed to the increased deformation strain energy resulting from MDF, which can facilitate the formation of fine $MgZn_2$ phases and the growth of the pre-existing $MgZn_2$ particles, during extrusion process.

(3) The tensile properties of the TiC_p/Mg−4Zn−0.5Ca nanocomposite subjected to MDF+EX multi-step deformation are improved relative to the as-extruded nanocomposite. The 3MDF310+EX nanocomposite exhibits excellent mechanical properties and its YS, UTS and EL are ~404 MPa, ~450.3 MPa and ~5.2%, respectively.

(4) Compared with the as-extruded or 3MDF270+EX nanocomposites, the DRXed grain is refined while the volume fraction of $MgZn_2$ phases is greatly increased for the 3MDF310+EX nanocomposite, leading to higher strengthening effects through grain refinement and Orowan strengthening.

References

[1] YANG L, HOU H, ZHAO Y H, YANG X M. Effect of applied pressure on microstructure and mechanical properties of Mg−Zn−Y quasicrystal-reinforced AZ91D magnesium matrix composites prepared by squeeze casting [J]. Transactions of Nonferrous Metals Society of China, 2015, 25(12): 3936−3943.

[2] ALAM M E, HAN S, NGUYEN Q B, HAMOUDA A M S, GUPTA M. Development of new magnesium based alloys and their nanocomposites [J]. Journal of Alloys and Compounds, 2011, 509: 8522−8529.

[3] SUN Y H, WANG R C, PENG C Q, FENG Y, YANG M. Recent progress in Mg−Li matrix composites [J]. Transactions of Nonferrous Metals Society of China, 2019, 29(1): 1−14.

[4] LIU W Q, WANG X J, HU X S, WU K, ZHENG M Y. Effects of hot rolling on microstructure, macrotexture and mechanical properties of pre-extruded AZ31/SiC nanocomposite sheets [J]. Materials Science and Engineering A, 2017, 683: 15−23.

[5] NIE K B, GUO Y C, DENG K K, KANG X K. High strength TiC_p/Mg−Zn−Ca magnesium matrix nanocomposites with improved formability at low temperature [J]. Journal of Alloys and Compounds, 2019, 792: 267−278.

[6] AYDIN F, SUN Y, TURAN M E. Influence of TiC content on mechanical, wear and corrosion properties of hot-pressed AZ91/TiC composites [J]. Journal of Composite Materials, 2020, 54(2): 141−152.

[7] GOH C S, WEI J, LEE L C, GUPTA M. Properties and deformation behaviour of Mg−Y_2O_3 nanocomposites [J]. Acta Materialia, 2007, 55: 5115−5121.

[8] AYDIN F, SUN Y, AHLATCI H, TUREN Y. Investigation of microstructure, mechanical and wear behavior of B_4C particulate reinforced magnesium matrix composites by powder metallurgy [J]. Transactions of the Indian Institute of Metals, 2018, 71(4): 873−882.

[9] SHEN M J, YING W F, WANG X J, ZHANG M F, WU K. Development of high performance magnesium matrix nanocomposites using nano-SiC particulates as reinforcement [J]. Journal of Materials Engineering and Performance, 2015, 24: 3798−3807.

[10] NIE K B, WANG X J, WU K, XU L, ZHENG M Y, HU X S. Processing, microstructure and mechanical properties of magnesium matrix nanocomposites fabricated by semisolid stirring assisted ultrasonic vibration [J]. Journal of Alloys and Compounds, 2011, 509: 8664−8669.

[11] ZENGIN H, TUREN Y, TURAN M E, AYDIN F. Evolution of microstructure, residual stress, and tensile properties of Mg−Zn−Y−La−Zr magnesium alloy processed by extrusion [J]. Acta Metallurgica Sinica (English Letters), 2019, 32: 1309−1319.

[12] SHEN M J, WANG X J, ZHANG M F, HU X S, ZHENG M Y, WU K. Fabrication of bimodal size SiC_p reinforced AZ31B magnesium matrix composites [J]. Materials Science and Engineering A, 2014, 601: 58−64.

[13] ZHANG Y, CHEN X Y, LIU Y L, LI X P. Microstructure and mechanical properties of as-extruded Mg−Sn−Zn−Ca alloy with different extrusion ratios [J]. Transactions of Nonferrous Metals Society of China, 2018, 28(11): 2190−2198.

[14] NIE K B, WANG X J, XU F J, WU K, ZHENG M Y. Microstructure and tensile properties of SiC nanoparticles reinforced magnesium matrix composite prepared by multidirectional forging under decreasing temperature conditions [J]. Materials Science and Engineering A, 2015, 639: 465−473.

[15] KHOSROSHAHI H K, SANIEE F F, ABEDI H R. Mechanical properties improvement of cast AZ80 Mg alloy/nano-particles composite via thermomechanical processing [J]. Materials Science and Engineering A, 2014, 595: 284−290.

[16] NIE K B, WANG X J, XU L, WU K, HU X S, ZHENG M Y. Influence of extrusion temperature and process parameter on microstructures and tensile properties of a particulate reinforced magnesium matrix nanocomposite [J]. Materials & Design, 2012, 36: 199−205.

[17] NIE K B, DENG K K, WANG X J, WANG T, WU K. Influence of SiC nanoparticles addition on the microstructural evolution and mechanical properties of AZ91 alloy during isothermal multidirectional forging [J]. Materials Characterization, 2017, 124: 14−24.

[18] DENG K K, WANG X J, GAN W M, WU Y W, NIE K B, WU K, ZHENG M Y, BROKMEIER H G. Isothermal forging of AZ91 reinforced with 10vol.% silicon carbon particles [J]. Materials Science and Engineering A, 2011, 528: 1707−1712.

[19] ZHU S Z, LUO T J, ZHANG T A, LIU Y T, YANG Y S. Effects of extrusion and heat treatments on microstructure and mechanical properties of Mg−8Zn−1Al−0.5Cu−0.5Mn alloy [J]. Transactions of Nonferrous Metals Society of China, 2017, 27(1): 73−81.

[20] TONG L B, ZHANG J B, ZHANG Q X, JIANG Z H, XU C, KAMADO S, ZHANG D P, MENG J, CHENG L R, ZHANG H J. Effect of warm rolling on the microstructure, texture and mechanical properties of extruded Mg−Zn−Ca−Ce/La alloy [J]. Materials Characterization, 2016, 115: 1−7.

[21] MATSUBARA K, MIYAHARA Y, HORITA Z, LANGDON T G. Developing superplasticity in a magnesium alloy through a combination of extrusion and ECAP [J]. Acta

Materialia, 2003, 51: 3073−3084.

[22] QIAO X G, YING T, ZHENG M Y, WEI E D, WU K, HU X S, GAN W M, BROKMEIER H G, GOLOVIN I S. Microstructure evolution and mechanical properties of nano-SiC_p/AZ91 composite processed by extrusion and equal channel angular pressing (ECAP) [J]. Materials Characterization, 2016, 121: 222−230.

[23] WU K, DENG K K, NIE K B, WU Y W, WANG X J, HU X S, ZHENG M Y. Microstructure and mechanical properties of SiC_p/AZ91 composite deformed through a combination of forging and extrusion process [J]. Materials & Design, 2010, 31: 3929−3932.

[24] NIE K B, GUO Y C, DENG K K, KANG X K. Microstructure and mechanical properties of TiC_p/Mg−4Zn−0.5Ca nanocomposite in different processing conditions [J]. Materials Research Express, 2019, 6(6): 066525.

[25] KANG J W, WANG C J, DENG K K, NI K B E, BAI Y, LI W J. Microstructure and mechanical properties of Mg−4Zn−0.5Ca alloy fabricated by the combination of forging, homogenization and extrusion process [J]. Journal of Alloys and Compounds, 2017, 720: 196−206.

[26] ZHU Z H, NIE K B, DENG K K, HAN J G, Fabrication of biodegradable magnesium matrix composite with ultrafine grains and high strength by adding TiC nanoparticles to Mg−1.12Ca−0.84Zn−0.23Mn (at.%) alloy [J]. Materials Science and Engineering C, 2020, 107: 110360.

[27] PARAMSOTHY M, CHAN J, KWOK R, GUPTA M. Adding TiC nanoparticles to magnesium alloy ZK60A for strength/ductility enhancement [J]. Journal of Nanomaterials, 2011, 2011: 1−9.

[28] NIE K B, WANG X J, XU L, WU K, HU X S, ZHENG M Y. Effect of hot extrusion on microstructures and mechanical properties of SiC nanoparticles reinforced magnesium matrix composite [J]. Journal of Alloys and Compounds, 2012, 512: 355−360.

[29] PARK S H, KIM H S, BAE J H, YIM C D, YOU B S. Improving the mechanical properties of extruded Mg−3Al−1Zn alloy by cold pre-forging [J]. Scripta Materialia, 2013, 69: 250−253.

[30] JIANG M G, XU C, NAKATA T, YAN H, CHEN R S, KAMADO S. Enhancing strength and ductility of Mg−Zn−Gd alloy via slow-speed extrusion combined with pre-forging [J]. Journal of Alloys and Compounds, 2017, 694: 1214−1223.

[31] WANG Z, ZHOU Y, LI Y Z, WANG F, LIU Z, MAO P L, JIANG X P. Hot tearing behaviors and in-situ thermal analysis of Mg−7Zn−*x*Cu−0.6Zr alloys [J]. Transactions of Nonferrous Metals Society of China, 2018, 28(8): 1504−1513.

[32] DING Z B, ZHAO Y H, LU R G, YUAN M N, WANG Z J, LI H J, HOU H. Effect of Zn addition on microstructure and mechanical properties of cast Mg−Gd−Y−Zr alloys [J]. Transactions of Nonferrous Metals Society of China, 2019, 29(4): 722−734.

[33] GUO K Y, XU C, LIN X P, YE J, ZHANG C, HUANG D. Microstructure and strengthening mechanism of Mg−5.88Zn−0.53Cu−0.16Zr alloy solidified under high pressure [J]. Transactions of Nonferrous Metals Society of China, 2020, 30(1): 99−109.

[34] NIE K B, ZHU Z H, DENG K K, WANG T, HAN J G. Hot Deformation behavior and processing maps of SiC nanoparticles and second phase synergistically reinforced magnesium matrix composites [J]. Nanomaterials, 2019, 19(1): 57.

[35] ZHANG C, WU L, ZHAO Z L, XIE Z H, HUANG G S, LIU L, JIANG B, ATRENS A, PAN F S. Effect of Li content on microstructure and mechanical property of Mg−*x*Li−3(Al−Si) alloys [J]. Transactions of Nonferrous Metals Society of China, 2019, 29(12): 2506−2513.

[36] TONG L B, ZHENG M Y, CHANG H, HU X S, WU K, XU S W, KAMADO S, KOJIMA Y. Microstructure and mechanical properties of Mg−Zn−Ca alloy processed by equal channel angular pressing [J]. Materials Science and Engineering A, 2009, 523: 289−294.

[37] OUYANG S J, LIU W C, WU G H, JI H, GAO Z K, PENG X, LI Z Q, DING W J. Microstructure and mechanical properties of as-cast Mg−8Li−*x*Zn−*y*Gd (*x*=1, 2, 3, 4; *y*=1, 2) alloys [J]. Transactions of Nonferrous Metals Society of China, 2019, 29(6): 1211−1222.

[38] YU H H, XIN Y C, WANG M Y, LIU Q. Hall−Petch relationship in Mg alloys: A review [J]. Journal of Materials Science & Technology, 2018, 34(2): 248−256.

[39] WANG F L, BHATTACHARYYA J J, AGNEW S R. Effect of precipitate shape and orientation on Orowan strengthening of non-basal slip modes in hexagonal crystals, application to magnesium alloys [J]. Materials Science and Engineering A, 2016, 666: 114−122.

[40] PAN H C, KANG R, LI J R, XIE H B, ZENG Z R, HUANG Q Y, YANG C L, REN Y P, QIN G W. Mechanistic investigation of a low-alloy Mg−Ca-based extrusion alloy with high strength–ductility synergy [J]. Acta Materialia, 2020, 186: 278−290.

[41] LIU K, LIU J X, LI S B, WANG Z H, DU W B, WANG Q F. Effects of secondary phases on texture and mechanical properties of as-extruded Mg−Zn−Er alloys [J]. Transactions of Nonferrous Metals Society of China, 2018, 28(5): 890−895.

[42] PAN H, QIN G, HUANG Y, REN Y, SHA X, HAN X, LIU Z Q, LI C, WU X, CHEN H, HE C, CHAI L, WANG Y, NIE J F. Development of low-alloyed and rare-earth-free magnesium alloys having ultra-high strength [J]. Acta Materialia, 2018, 149: 350−363.

[43] WU Y P, XIONG H Q, JIA Y Z, XIE X H, LI G F. Microstructure, texture and mechanical properties of Mg−8Gd−4Y−1Nd−0.5Zr alloy prepared by pre-deformation annealing, hot compression and ageing [J]. Transactions of Nonferrous Metals Society of China, 2019, 29(5): 976−983.

[44] GUO Y C, NIE K B, KANG X K, DENG K K, HAN J G, ZHU Z H. Achieving high-strength magnesium matrix nanocomposite through synergistical effect of external hybrid (SiC+TiC) nanoparticles and dynamic precipitated phase [J]. Journal of Alloys and Compounds, 2019, 771: 847−856.

[45] DENG K, SHI J, WANG C, WANG X, WU Y, NIE K, WU K. Microstructure and strengthening mechanism of bimodal size particle reinforced magnesium matrix composite [J]. Composites (Part A): Applied Science and Manufacturing, 2012, 43(8): 1280−1284.

[46] ZHANG H, WANG W Y, WANG J G, RONG J, ZHA M, WANG C, MA P K, JIANG Q C. The synergy effect of fine and coarse grains on enhanced ductility of bimodal-structured Mg alloys [J]. Journal of Alloys and Compounds, 2019, 780: 312−317.

[47] NIE K B, ZHU Z H, MUNROE P, DENG K K, HAN J G. The effect of Zn/Ca ratio on the microstructure, texture and mechanical properties of dilute Mg−Zn−Ca−Mn alloys that exhibit superior strength [J]. Journal of Materials Science, 2020, 55: 3588−3604.

联合多向锻造与挤压变形 TiC 纳米颗粒增强 Mg−Zn−Ca 基复合材料的组织与力学性能

聂凯波[1]，朱智浩[1]，Paul MUNROE[2]，邓坤坤[1]，郭亚超[1]

1. 太原理工大学 材料科学与工程学院，太原 030024；

2. School of Materials Science and Engineering, University of New South Wales, Sydney, NSW 2052, Australia

摘　要：采用多向锻造(MDF)和挤压(EX)相结合工艺对 TiC 纳米颗粒增强 Mg−4Zn−0.5Ca 基纳米复合材料进行变形。与仅单一 MDF 相比，经 MDF+EX 变形后纳米复合材料的晶粒尺寸显著减小。当 MDF 温度为 270 °C 时，随 MDF 道次的增加，经 EX 变形后再结晶(DRX)晶粒的平均尺寸逐渐增大；而当 MDF 温度为 310 °C 时，经 EX 变形后 DRX 晶粒的平均尺寸显著减小。经 MDF+EX 多步变形后纳米复合材料中同时出现细小和粗大的 $MgZn_2$ 相，这些 $MgZn_2$ 相的体积分数随 EX 前 MDF 道次的增加而逐渐增大。对温度为 310 °C 经 3 道次 MDF 后的纳米复合材料进行 EX，其屈服强度、极限抗拉强度和伸长率分别达到 ~404 MPa，~450.3 MPa 和 ~5.2%。这主要与 MDF+EX 多步变形后晶粒细化强化及 $MgZn_2$ 析出相引起的 Orowan 强化有关。

关键词：镁基纳米复合材料；多步变形；多向锻造；力学性能；$MgZn_2$ 相

(Edited by Xiang-qun LI)